MNRAS 000, 1–13 (2020) Preprint 1 December 2023 Compiled using MNRAS LATEX style file v3.0

# Model-independent discovery prospects for primordial black holes at LIGO

Benjamin V. Lehmann,[1,2]★ Stefano Profumo,[1,2]† and Jackson Yant[1,2,3]‡
[1]Department of Physics, University of California Santa Cruz, 1156 High St., Santa Cruz, CA 95064, USA
[2]Santa Cruz Institute for Particle Physics, 1156 High St., Santa Cruz, CA 95064, USA
[3]Department of Physics and Astronomy, Dartmouth College, Hanover, NH 03755, USA

arXiv:2007.00021v1 [astro-ph.CO] 30 Jun 2020

Accepted XXX. Received YYY; in original form ZZZ

**ABSTRACT**

Primordial black holes may encode the conditions of the early universe, and may even constitute a significant fraction of cosmological dark matter. Their existence has yet to be established. However, black holes with masses below $\sim 1\,M_\odot$ cannot form as an endpoint of stellar evolution, so the detection of even one such object would be a smoking gun for new physics, and would constitute evidence that at least a fraction of the dark matter consists of primordial black holes. Gravitational wave detectors are capable of making a definitive discovery of this kind by detecting mergers of light black holes. But since the merger rate depends strongly on the shape of the black hole mass function, it is difficult to determine the potential for discovery or constraint as a function of the overall abundance of black holes. Here, we directly maximize and minimize the merger rate to connect observational results to the actual abundance of observable objects. We show that LIGO can discover mergers of light primordial black holes within the next decade even if such black holes constitute only a very small fraction of dark matter. A single merger event involving such an object would (i) provide conclusive evidence of new physics, (ii) establish the nature of some fraction of dark matter, and (iii) probe cosmological history at scales far beyond those observable today.

**Key words:** black hole mergers — gravitational waves — dark matter — methods: analytical — methods: numerical

## 1 INTRODUCTION

The detection of black hole binaries with LIGO (Abbott et al. 2016b,d, 2017b,c,g, 2019a, 2020b,a) has heralded a new era in probing the nature and behavior of compact objects in our universe. In the past several years, gravitational wave detectors have directly confirmed the existence of black holes (Abbott et al. 2016a), provided powerful tests of general relativity (Abbott et al. 2016c), and ushered in the era of multi-messenger astronomy (Abbott et al. 2017e,f). But as gravitational wave observatories continue to probe the black hole population, they are poised to make yet another significant discovery: mergers may provide direct evidence for the existence of primordial black holes.

Primordial black holes (PBH) may form in the early universe without stellar progenitors, and they have been intensely studied as potential probes of cosmology and high-energy physics (see e.g. Carr 2003; Khlopov 2010; Calmet et al. 2014). In the simplest scenario, PBH are formed by the gravitational collapse of large density perturbations on small scales (Zel'dovich & Novikov 1967; Hawking 1971). Other formation channels, such as gravitational collapse in a dark sector (Shandera et al. 2018), or the collapse of another compact object due to new physics (see e.g. de Lavallaz & Fairbairn 2010), can also result in observable black holes of non-stellar origin. Since the interactions of massive PBH are dominated by gravitation, and since a collection of black holes is fluid-like on sufficiently large scales, PBH are a natural candidate for cosmological dark matter, a possibility that was recognized shortly after their existence was postulated (Chapline 1975).

In the decades since, the PBH population has been constrained by various astrophysical and cosmological means, but never fully ruled out as a dark matter candidate (Carr et al. 2010, 2016, 2020; Carr & Kuhnel 2020; Lehmann et al. 2018). Soon after the first observation of a binary black hole merger, Bird et al. (2016) and Sasaki et al. (2016) pointed out that the merger rate implied by LIGO's discovery is potentially consistent with a population of PBH accounting for all of dark matter, advancing the possibility that the two black holes involved had a primordial origin—and, indeed, that LIGO had detected dark matter.

Regardless of the relation to cosmological dark matter, the confirmation of a primordial origin for any black hole would carry great implications. Such a population might probe primordial fluctuations at scales well beyond the reach of other experiments, providing a

★ E-mail: blehmann@ucsc.edu
† E-mail: profumo@ucsc.edu
‡ E-mail: jackson.yant.phys@gmail.com

© 2020 The Authors

unique window into early cosmology, and an unprecedented test of physics at extremely high energies. The primordial-origin scenario for the black holes observed at LIGO has thus been discussed heavily in the literature. Interestingly, the masses and spins of the black hole binaries detected by LIGO are unexpected in the simplest astrophysical formation models (see e.g. Gerosa & Berti 2017), sparking additional interest in a PBH interpretation. It may even be possible to distinguish between stellar- and primordial-origin models statistically in the coming years by measuring the distribution of the binaries' spin parameters (Fernandez & Profumo 2019). However, this is complicated by uncertainties in stellar evolution models, and even in the most optimistic case, it will be difficult to positively establish a non-stellar origin, especially for a subcomponent of the black hole population.

But there is one clean signal which could clearly indicate the primordial origin of a specific black hole: a low mass. Stellar evolution models predict that black holes form only when a star's mass is sufficient for the gravitational force to overcome degeneracy pressure. Thus, black holes with a stellar origin must have a mass no lower than the Chandrasekhar limit of $1.4\,M_\odot$ (Chandrasekhar 1931). A black hole with a mass below $\sim 1\,M_\odot$ must have a non-stellar origin, and the detection of even one such object would be a clear smoking gun of new physics, as was already pointed out by Chapline (1975). In principle, LIGO may be sensitive to mergers of black holes well below this scale, so LIGO and other gravitational wave observatories are uniquely capable of directly establishing the existence of primordial black holes.

Indeed, some gravitational wave detections have already come tantalizingly close to furnishing such a discovery. The latest hint comes from the recently-announced GW190814 (Abbott et al. 2020c), apparently involving a compact object at $2.6\,M_\odot$, in what was expected to be a mass gap in the population of neutron stars and stellar-origin black holes (Bailyn et al. 1998; Ozel et al. 2010; Farr et al. 2011; Ozel et al. 2012). Additionally, the nature of the compact objects involved in GW170817 (Abbott et al. 2017d) is uncertain: while the identification of an associated kilonova (Soares-Santos et al. 2017) strongly indicates that one of the merging objects was a neutron star, the second compact object might also be a light $O(1\,M_\odot)$ black hole, with likelihood as large as 40% (see e.g. Coughlin & Dietrich 2019).

Given the potential for discovery, the LIGO Collaboration has conducted initial searches for mergers of light PBH (Abbott et al. 2005, 2019b), with null results thus far. But interpreting these null results as constraints on the PBH population requires a model to connect the abundance and mass distribution of PBH to the rate of observed mergers. Theoretical uncertainties in the merger rate complicate such an analysis, with notable recent progress by Vaskonen & Veermäe (2020). Even so, most previous work has assumed that the PBH mass function is monochromatic, i.e., that all PBH have a single mass. This greatly simplifies the problem, but is likely unrealistic: in most formation models, PBH have an extended mass distribution with a lognormal or power-law shape (Carr et al. 2016). In some scenarios, the mass distribution can even be multimodal (Carr & Kuhnel 2019).

A bias-free interpretation of LIGO results requires that we allow for some freedom in the shape of the mass function. This motivates the approach taken by Chen & Huang (2019), who analyze prospects for the detection of light black holes under the assumption that the mergers observed thus far have a primordial origin. To further complicate matters, the mass distribution is subject to various observational constraints across the mass spectrum, which impose additional restrictions on the space of mass functions. The uncertainty in the merger rate arising from the shape of the mass function means that it is difficult to describe prospects for either constraints on or discovery of a PBH population at gravitational wave observatories in a model-independent fashion.

In this work, we use numerical methods to translate null searches at gravitational wave observatories into constraints on the properties of the PBH population and discovery prospects for light black holes. In particular, we show that if only a small fraction of the PBH population lies in the mass window of interest, then freedom in the mass function translates to a significant gap between the *constraint* potential and the *discovery* potential, corresponding to the most pessimistic and optimistic calculations of the merger rate, respectively. We show that LIGO can establish the existence of primordial black holes even if the abundance of such objects in the mass range of interest is far below the level of the prospective constraint. Our results provide the first model-independent gravitational wave constraints on the light black hole population, and show that there is considerable opportunity for their discovery at LIGO.

This paper is organized as follows. In section 2, we review the calculation of the merger rate and establish analytical expectations for the shapes of mass functions which maximize and minimize the merger rate. In section 3, we introduce our numerical procedure and detail the inclusion of other observational constraints. We present our numerical results in section 4, and we discuss the implications and conclude in section 5.

Notationally, we will say that a black hole is "light" if it has a mass below $1\,M_\odot$, and we will say that a black hole is "detectable" if it has a mass large enough to be observable by LIGO, a condition we will detail in subsequent sections. We will refer to light black holes as "primordial", although, as we have mentioned, there are other new physics scenarios which may also result in the formation of observable black holes without stellar progenitors. Our interest is in light black holes which are "detectable and primordial", which we will abbreviate as "DPBH". We will say that such black holes lie in the "DP" mass range.

## 2 THE MERGER RATE OF DPBH

To establish the most optimistic discovery prospects, and the most pessimistic constraint potential, it is necessary to consider, respectively, the maximum and minimum merger rates that can be produced with a fixed abundance of PBH. We will perform this optimization numerically in the following sections, but first, we discuss the calculation of the merger rate and explore a few benchmark cases analytically.

The merger rate of primordial black holes has been studied by many authors (Bird et al. 2016; Mandic et al. 2016; Sasaki et al. 2016; Clesse & García-Bellido 2017; Raidal et al. 2017; Chen & Huang 2018; Vaskonen & Veermäe 2020), and while predictions of the rate are still subject to some uncertainties, the theoretical formalism has improved considerably in recent years. In particular, Raidal et al. (2017) and Chen & Huang (2018) have studied the merger rate for extended mass functions, and established predictions for the merger rate as a function of the component masses. The formation of merging primordial black hole binaries is quite different from the stellar case, so we will shortly review the derivation of the merger rate and the attendant physics.

Throughout the following sections, we will denote the mass function by $\psi$. Denoting the PBH number density for masses up to $m$ by $n(m)$, the mass function is defined by $\psi(m) \propto m\,\mathrm{d}n/\mathrm{d}m$ with

the normalization condition

$$\int \mathrm{d}m\, \psi(m) = \frac{\Omega_{\rm PBH}}{\Omega_{\rm DM}} \equiv f_{\rm PBH}. \tag{1}$$

### 2.1 The detectable mass range

A key component of estimating the DPBH merger rate is defining exactly what is meant by detectability. In previous studies of DPBH mergers, a threshold is generally set at a mass of order $\sim 0.1\,\mathrm{M}_\odot$, and mergers of black holes below the threshold mass are assumed to be undetectable. We must do the same in this work, for reasons we will explain shortly. For the moment, note that this is a reasonable approximation, especially because gravitational wave detectors trigger on the basis of a bank of template waveforms. Thus, even if LIGO is potentially sensitive to mergers of lighter objects, a detection will not be made if no matching template has been computed. In typical operation, LIGO uses no templates with combined binary masses below $2\,\mathrm{M}_\odot$ (Magee et al. 2018), and even past searches for light black hole mergers have used a minimum template mass of $0.4\,\mathrm{M}_\odot$ (Abbott et al. 2005, 2019b).

Neglecting templates, LIGO is potentially sensitive to mergers of very light black holes, with one important caveat: the lighter the binary, the closer it must be in order for the merger to be detectable. Thus, LIGO probes a different effective volume $V_{\rm eff}(m_1, m_2)$ for each pair of component masses $(m_1, m_2)$. Given a particular mass function $\psi$, the total DPBH merger rate $R_{\rm DP}$ must then be written in the form

$$R_{\rm DP}(\psi) = \int_{\rm DP^2} \mathrm{d}m_1\, \mathrm{d}m_2\, \mathcal{R}(m_1, m_2) V_{\rm eff}(m_1, m_2), \tag{2}$$

where $\mathcal{R}(m_1, m_2)$ is the differential merger rate per unit volume for binaries with component masses $(m_1, m_2)$, and $\int_{\rm DP^2}$ denotes an integral only over pairs of masses in the DP regime. We make the simplifying approximation that the sensitive volume depends only on the chirp mass of the binary, $M_c$, and not on the individual component masses, so that $V_{\rm eff}(m_1, m_2) = V_{\rm eff}(M_c(m_1, m_2))$. This approximation has been explicitly validated by Abbott et al. (2019b). We take the sensitive volume at fixed $M_c$ from Magee et al. (2018). As noted in that work, there are potentially significant computational costs to give LIGO sensitivity to very low-mass binaries. Still, we optimistically adopt the largest possible sensitive volume derived therein. Note that we neglect any impact of binary spin on detectability.

We still need to define the domain of the integral in eq. (2). To meaningfully probe the abundance of light PBH, we will ultimately be interested in speaking of the abundance in a narrow mass range, neither too massive to be clearly primordial, nor too light to be typically detectable, but just right (see e.g. Hassall 1904). To that end, we will define two thresholds $m_{\rm DP}^{\rm min}$ and $m_{\rm DP}^{\rm max}$. For single masses, we will say $m \in \mathrm{DP}$ if $m_{\rm DP}^{\rm min} \leq m \leq m_{\rm DP}^{\rm max}$. For pairs of masses, we will say that $(m_1, m_2) \in \mathrm{DP}^2$ if $m_{\rm DP}^{\rm min} \leq \min\{m_1, m_2\} \leq m_{\rm DP}^{\rm max}$, i.e., if

(i) *both* $m_1$ and $m_2$ are above $m_{\rm DP}^{\rm min}$, and
(ii) *at least one* of $m_1$ and $m_2$ is below $m_{\rm DP}^{\rm max}$.

We will fix $m_{\rm DP}^{\rm max} = 1\,\mathrm{M}_\odot$ and $m_{\rm DP}^{\rm min} = 0.1\,\mathrm{M}_\odot$ throughout our analysis. We have investigated the consequences of choosing $m_{\rm DP}^{\rm min} = 0.01\,\mathrm{M}_\odot$, and found that there is very little impact on the qualitative outcomes of our analysis: while choosing a lower threshold threshold extends the opportunity for discovery if PBH only exist at lower masses, extant gravitational wave detectors are relatively poorly suited to probe such a population.

In order to meaningfully discuss constraints on the DPBH population, we define the DP ratio by

$$r_{\rm DP} = \frac{1}{f_{\rm PBH}} \int_{m_{\rm DP}^{\rm min}}^{m_{\rm DP}^{\rm max}} \mathrm{d}m\, \psi(m). \tag{3}$$

This is the mass fraction of PBH with masses between $m_{\rm DP}^{\rm min}$ and $m_{\rm DP}^{\rm max}$. Note the use of $r$ ("ratio") rather than $f$ to avoid confusion with $\Omega_{\rm DP}/\Omega_{\rm DM}$, as with $f_{\rm PBH}$. We instead define $f_{\rm DP} \equiv r_{\rm DP} f_{\rm PBH}$.

Ultimately, we will evaluate maximum and minimum merger rates as a function of both $f_{\rm PBH}$ and $r_{\rm DP}$ simultaneously. This is a convenient parametrization for discussing constraints on the mass function, since despite the very simple form of the two parameters, they encode key information about the abundance of PBH in general and the abundance of light black holes in particular. This is also one of the reasons for imposing a strict cutoff at low masses: one might contend that lighter black holes, with masses below our $m_{\rm DP}^{\rm min}$, are also detectable, albeit in a smaller volume. This may indeed be the case, but including such mergers would make the parametrization discussed here difficult to interpret in relation to the merger rate: black holes just below $m_{\rm DP}^{\rm min}$ would contribute to the DP merger rate, but not to $r_{\rm DP}$.

We note that LIGO is not equipped with templates for our entire DP window during its regular operation, and a search with black hole masses below $0.2\,\mathrm{M}_\odot$ has not been conducted to date. Moreover, previous searches have targeted mergers between two light black holes, with templates only below $4\,\mathrm{M}_\odot$ in total binary mass. Thus, the constraints we draw in this work are prospective, assuming that an extended search is conducted on archival or future data. As we will show, such searches are well-motivated both for pairs of light black holes and for mergers of light black holes with heavy partners. There is ample opportunity to discover primordial black holes even at abundances that cannot be fully constrained.

### 2.2 Estimating the merger rate

We now review the derivation of the merger rate in Raidal et al. (2017) and Chen & Huang (2018). First, we note that PBH binaries can form in two epochs: in the early universe, during radiation domination, and in the late universe, where close approaches can produce enough gravitational radiation to bind two black holes. The latter contribution is generally small, since typical relative velocities are large, meaning that the energy loss to gravitational radiation must be quite significant. There is a possible exception to this rule if the density contrast in the late universe is exceptionally large, $\delta_0 \gtrsim 10^{10}$, but this is much larger than most estimates, so we neglect that possibility. Thus, we consider only binaries formed in the early universe. Note that our calculation may not accurately describe new physics scenarios in which light black holes themselves form in the late universe.

We first review the merger rate as estimated by Raidal et al. (2017). Consider a PBH pair with masses $m_1$ and $m_2$. First, in order for the pair to decouple from the Hubble flow and have interactions dominated by their mutual gravitation, the average mass of the black holes should exceed the background mass in the volume between them, i.e., we require $\frac{1}{2}(m_1 + m_2) > \frac{4\pi}{3}\rho_{\rm bg} r^3$. Translating this into a condition on the separation of the two black holes, one finds that the comoving distance between them must fall below the scale

$$\tilde{x}(m_1, m_2)^3 = \frac{3}{4\pi} \frac{m_1 + m_2}{a_{\rm eq}^3 \rho_{\rm eq}}, \tag{4}$$

where $a_{\rm eq}$ and $\rho_{\rm eq}$ are the scale factor and density at matter-radiation

equality. A binary with comoving separation $x < \tilde{x}$ thus decouples from the Hubble flow when the scale factor is

$$a_{\rm dc} = a_{\rm eq}\left(\frac{x}{\tilde{x}}\right)^3. \tag{5}$$

After this point, the black holes' gravity dominates the evolution of the system. Barring a close approach, gravitational interactions between these two black holes and some third body of comparable mass are necessary to move the pair into a bound configuration. Thus, we suppose that there is third PBH with mass $m_3$ at a comoving distance $y$ from the first two. In this scenario, we form a binary with semi-major and semi-minor axes given by

$$r_a = \alpha x a_{\rm dc}, \qquad r_b = \beta\frac{2m_3}{m_1+m_2}\left(\frac{x}{y}\right)^3 r_a, \tag{6}$$

for two $O(1)$ constants $\alpha$ and $\beta$. We take $\alpha = \beta = 1$ for the remainder of this discussion. Assuming that there is no mechanism for hardening the binary apart from gravitational radiation, the coalescence time can then be estimated as

$$\tilde{\tau}(m_1, m_2, m_3)\left(\frac{x}{\tilde{x}(m_1,m_2)}\right)^{37}\left(\frac{y}{\tilde{x}(m_1,m_2)}\right)^{-21}, \tag{7}$$

where $\tilde{\tau}$ is the maximal coalescence time, given by

$$\tilde{\tau}(m_1, m_2, m_3) = \frac{348}{85}\frac{\alpha^4\beta^7 a_{\rm eq}^4 m_3^7 \tilde{x}(m_1,m_2)^4}{G^3 m_1 m_2 (m_1+m_2)^8}. \tag{8}$$

Here we have established the coalescence time for a single binary assuming a set of masses and initial separations. Distributions of these parameters can be derived from the mass function, leading to a distribution of coalescence times as a function of the component masses. Differentiating this distribution at the present time leads to the current merger rate. For brevity, we define $\tilde{m}(\psi) = 1/\int {\rm d}m\,\psi(m)/m$. The number density of PBH at the mass of interest is accounted for through the factor $\tilde{N}(\psi;\ m_1, m_2) = \delta_{\rm dc}\Omega_{\rm DM,eq}(m_1+m_2)/\tilde{m}(\psi)$, where $\delta_{\rm dc}$ is the density contrast at the time of decoupling. We then define

$$\mathcal{G}(\psi;\ m_1, m_2, m_3) = \Gamma\left(\frac{58}{37},\ \frac{\tilde{N}(\psi;\ m_1,m_2)\,t^{3/16}}{\tilde{\tau}(m_1,m_2,m_3)^{3/16}}\right) - \Gamma\left(\frac{58}{37},\ \frac{\tilde{N}(\psi;\ m_1,m_2)\,t^{-1/7}}{\tilde{\tau}(m_1,m_2,m_3)^{-1/7}}\right), \tag{9}$$

and the present-day differential merger rate between black holes with masses $m_1$ and $m_2$ is given by

$$\mathcal{R}(m_1,m_2) = \frac{9\tilde{m}(\psi)^3\tilde{N}(\psi;\ m_1,m_2)^{\frac{53}{37}}}{296\pi\delta_{\rm dc}\tilde{x}(m_1,m_2)^3 t^{34/37}} \times\frac{\psi(m_1)\psi(m_2)}{m_1 m_2}\int {\rm d}m_3\,\frac{\mathcal{G}(\psi;\ m_1,m_2,m_3)}{\tilde{\tau}(m_1,m_2,m_3)^{3/37}}\frac{\psi(m_3)}{m_3}. \tag{10}$$

Notably, this estimate of the merger rate considers only the tidal torque due to one additional PBH external to the binary. This may present a problem when dealing with mass functions that span many decades, for which lighter black holes have relatively high number densities. Chen & Huang (2018) follow a similar line of argument, but the authors estimate the torque by integrating over the entire PBH population. It might be expected that this form of the merger rate is more reliable for extremely broad or multimodal mass functions, which we may well encounter in the course of our analysis. Thus, we use their merger rate in the course of our calculation, and we now briefly summarize their result. We define

$$\mu = \frac{2m_1m_2\left(\psi(m_1)+\psi(m_2)\right)}{(m_1+m_2)\left(m_1\psi(m_1)+m_2\psi(m_2)\right)} \tag{11}$$

and $n_T = \rho_c\Omega_{\rm DM,eq}\int {\rm d}m\,\psi(m)/m$, where the lower limit of integration is $\min\{m_1, m_2\}$. We additionally take $\langle x\rangle$ to be the average separation between black holes of mass $m_1$ and $m_2$, and define $\gamma_X$ by

$$\gamma_X = \left(\frac{85}{3}\frac{t m_1 m_2(m_1+m_2)\left(\psi(m_1)+\psi(m_2)\right)^4}{10^{-4}\left(\frac{3}{8\pi}\frac{m_1+m_2}{\rho_{\rm eq}(\psi(m_1)+\psi(m_2))}\right)^{4/3}X^{16/3}}\right)^{1/7} \times\frac{2(\psi(m_1)+\psi(m_2))\Omega_{\rm M}}{\Omega_{\rm DM}X}. \tag{12}$$

Then the probability distribution for the coalescence time is given by

$$\frac{{\rm d}P}{{\rm d}t} = \frac{1}{7\mu t}\int {\rm d}X\,\exp\left(-\frac{X}{\mu}\frac{4\pi}{3}\langle x\rangle^3 n_T\right)\frac{\gamma_X^2}{\left(1+\gamma_X^2\right)^{3/2}}, \tag{13}$$

and the present-day merger rate per unit volume is given differentially in the component masses by

$$\mathcal{R}(m_1,m_2) = \rho_c\Omega_{\rm M}\min\left(\frac{\psi(m_1)}{m_1},\ \frac{\psi(m_2)}{m_2}\right)\frac{{\rm d}P}{{\rm d}t}. \tag{14}$$

### 2.3 Analytical behavior of the merger rate

To establish constraint and discovery prospects, we will need to minimize and maximize the merger rate over the possible mass function shapes with some characteristic abundances held fixed. In particular, we will optimize the merger rate with $r_{\rm DP}$ and $f_{\rm PBH}$ held constant. For fixed $f_{\rm PBH}$, if the maximum merger rate falls below the LIGO sensitivity for a given value of $r_{\rm DP}$, this means that values of $r_{\rm DP}$ this low cannot be probed by LIGO, regardless of the form of the mass function. Alternately, if the minimum merger rate is detectable by LIGO, then this and higher values of $r_{\rm DP}$ can be ruled out by LIGO.

In general, the merger rate must be maximized or minimized numerically. However, to understand the dependence of the merger rate on the shape of the mass function, it is useful to consider a few simple benchmark cases in the absence of any observational constraints. For the moment, we neglect the mass dependence of the detector's sensitive volume.

First, consider a monochromatic mass function, $\psi(m) = f_1\delta(m-m_1)$. Formally, the quantities entering eq. (14) are not independently well-defined in this case, but we can take a mass function of the form

$$\psi_1(m) = f_1\Delta^{-1}\Theta(m-m_1)\Theta(m_1+\Delta-m) \tag{15}$$

and work in the limit $\Delta\to 0$. In this case, the total DP rate is simply the overall rate, as long as $m_1$ lies within the DP window. If $m_1$ is sufficiently small, the integrand of eq. (13) is dominated by values of $X$ where the exponential is very nearly 1. As pointed out by Chen & Huang (2018), the integral can then be evaluated approximately, which gives a rate $\mathcal{R}\propto m_1^{-32/37}$. A similar result can be derived for large $m_1$ by splitting the $X$ integral into two regimes, one in which the constant term in the denominator is dominant, and one in which it is subdominant. The integral can be evaluated analytically in each of the two regimes, and it can then be shown that $\mathcal{R}\propto m_1^{-26/21}$ at large $m_1$.

In particular, for a monochromatic mass function, decreasing $m_1$ increases the merger rate. Physically, this is simply because decreasing $m_1$ while holding $f_1$ constant increases the number density of black holes. In the absence of observational constraints, we

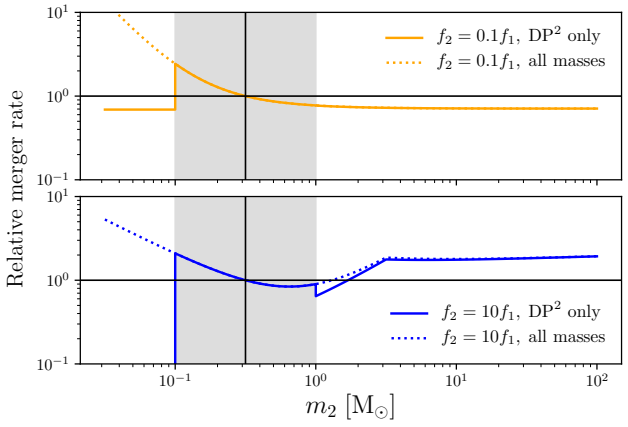



**Figure 1.** Merger rate for a dichromatic mass function, $\psi(m) = f_1\delta(m - m_1) + f_2\delta(m - m_2)$, relative to the monochromatic mass function $(f_1 + f_2)\delta(m - m_1)$. We fix $m_1 = 10^{-1/2}\mathrm{M}_\odot$, indicated by the black vertical line. This lies in the middle of the DP window, indicated by the shaded region. Dashed curves show the merger rate for pairs of all masses, while solid curves include only mergers in DP$^2$. The blue curve shows the case $f_2 = 10f_1$, i.e., where mergers of black holes of mass $m_2$ naively dominate. The orange curve shows the case $f_2 = 0.1f_1$, where the reverse is true. Depending on the relative amplitudes and positions of the two peaks, separating them can either enhance or suppress the merger rate (see text).

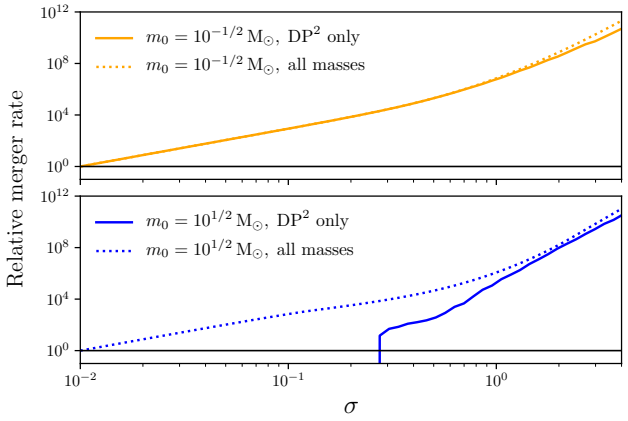



**Figure 2.** Relative merger rate as $\sigma$ is increased for a lognormal mass function with two different central masses. Dashed lines include all mergers, while solid lines include only DP$^2$ mergers. Curves are normalized relative to the all-inclusive merger rate at the lowest value of $\sigma$, i.e., the dashed lines are fixed to 1 at the left edge of the figure. For much of the range of $\sigma$ shown here, a large fraction of mergers lie in DP$^2$, so the solid and dashed lines lie very close. They begin to diverge at large $\sigma$ in both subplots, since much of the mass lies outside the DP window in this case. For the blue curve, the central mass lies outside the DP window, so the DP merger rate vanishes at small $\sigma$. In the limit $\sigma \to 0$, the lognormal mass function reduces to the monochromatic case.

therefore expect that the merger rate will be maximized when the mass function is peaked near the bottom of the DP window, and minimized when it is peaked near the top.

This is the simplest way in which the mass function can influence the merger rate. However, monochromatic mass functions are tightly constrained by observational bounds, so it is useful to understand the behavior of the merger rate for mass functions with non-negligible width. We first consider the simplest extension of the previous case: a bimodal mass function constructed as the sum of two monochromatic mass functions. We define

$$\psi_2(m) = f_1\delta(m - m_1) + f_2\delta(m - m_2), \tag{16}$$

where the Dirac delta is understood to be defined as in eq. (15).

For such a "dichromatic" mass function, there are three contributions to the merger rate, corresponding to mergers of black holes with masses $\{m_1, m_1\}$, $\{m_2, m_2\}$, and $\{m_1, m_2\}$. This gives rise to complicated behavior as the peaks are separated. Two benchmark cases are shown in fig. 1, with one peak fixed in the middle of the DP range and the other varying freely. In each panel, the merger rate is enhanced if the second peak is positioned at a low mass within the DP window, due to the enhanced number density. The DP merger rate (solid line) drops sharply as the mass of the second peak falls below the DP window, while the all-inclusive merger rate (dotted line) continues to increase.

Notice that as the second peak rises above the DP window, the drop in the DP merger rate is much less significant. This is because the presence of these more massive black holes still affects the DP merger rate in two ways: first, more massive black holes can still participate in the formation of light PBH binaries, and second, mergers of binaries with masses $\{m_1, m_2\}$ themselves contribute to the DP merger rate. These effects lead to non-trivial behavior of the dichromatic merger rate as a function of the two masses. For our purposes, we note that separating peaks in a dichromatic mass function can either increase or decrease the merger rate.

Finally, we consider a lognormal mass function, which is unimodal, but has a non-vanishing width. The lognormal mass function has the form

$$\psi_L(m) = \frac{f_{\mathrm{PBH}}}{\sqrt{2\pi}\sigma m}\exp\left(-\frac{1}{2}\left[\frac{\log(m/m_0)}{\sigma}\right]^2\right), \tag{17}$$

where $m_0$ corresponds to the central mass and $\sigma$ is the width of the distribution. Holding $\sigma$ fixed, the merger rate is increased by reducing $m_0$, as in the monochromatic case. If $m_0$ is fixed, and $\sigma$ is varied, then the merger rate is enhanced by increasing $\sigma$, i.e., broadening a sharp distribution locally increases the merger rate. This behavior is shown in fig. 2.

These benchmark scenarios indicate that a fairly broad mass function favoring lower masses will generally produce a higher merger rate, but in general, observational constraints will impose severe restrictions on the allowed shape of the mass function. Thus, the mass function which minimizes or maximizes the merger rate might indeed be a complicated multimodal function. In particular, the analysis of Lehmann et al. (2018) demonstrates that the maximum value of $f_{\mathrm{PBH}}$ consistent with observational constraints is attained by a multimodal mass function, corresponding to a superposition of monochromatic mass functions. Thus, it would not be surprising to find a similar behavior for mass functions which maximize the merger rate, particularly if $f_{\mathrm{PBH}}$ is fixed at a value where observational bounds strongly constrain the mass function. The benchmark scenarios in this section suggest that the merger rate will be minimized with sharply peaked and potentially multimodal mass functions.

To go further and to incorporate observational constraints will require numerical methods, which we take up in the following sections. Again, note that the discussion above has not accounted for any characteristics of the detector. In particular, we have neglected the mass dependence in the effective volume that an instrument such as LIGO can probe. Mergers of more massive black holes are ob-

servable in a larger effective volume, and this enhances the effective merger rate at higher PBH masses, competing with the enhancement in number density at lower masses. We will include this effect in our numerical treatment.

## 3 CONSTRAINTS AND OPTIMIZATION

In this section, we detail the numerical procedure that we use to optimize the merger rate. First, we discuss the constraints that we impose on the black hole mass function.

Since the allowed values of the merger rate depend on the allowed forms of the PBH mass function, observational constraints which restrict the form of the mass function correspondingly restrict the merger rate. Thus, the minimum or maximum merger rate is dependent not only on $f_{\rm PBH}$ and $r_{\rm DP}$, but also on the chosen set of observational constraints. The full set of observational constraints we use in this work is shown in figs. 4 and 5, with descriptions in the captions. We demonstrate the behavior of the maximum and minimum merger rates both with and without the constraints imposed on the mass function by these observational bounds.

Note that there are many other observables that may place constraints on the PBH population, such as supernova lensing (Zumalacarregui & Seljak 2018), dynamical effects (Monroy-Rodríguez & Allen 2014; Brandt 2016; Koushiappas & Loeb 2017), and destruction of white dwarf stars (Graham et al. 2015) and neutron stars (Capela et al. 2013). (See Carr et al. (2016, 2020); Carr & Kuhnel (2020) for reviews.) These constraints are subject to additional uncertainties, and including them does not change our qualitative conclusions. The qualitatively important features are the relative strength of the constraints at masses above and below the DP window, and the fact that there is a gap in the constraints at low masses. The latter allows for large values of $f_{\rm PBH}$ when $r_{\rm DP}$ is small. This gap has attracted considerable attention since lensing constraints at low masses were shown to be ineffective (Inomata et al. 2018; Katz et al. 2018; Montero-Camacho et al. 2019; Sugiyama et al. 2020; Smyth et al. 2020), and it is possible that new constraints developed in this region will influence our results.

We introduce one important observable beyond the constraints plotted in figs. 4 and 5: the stochastic gravitational wave background (SGWB, Abbott et al. 2009, 2017a). A population of black holes merging over cosmic time produces an accumulated background of gravitational radiation that can be detected by LIGO. Since the SGWB depends in detail on the shape of the mass function, it must be treated differently from the other constraints. However, it is essential that we include this constraint, since it has been shown that merging DPBH in particular can make a significant contribution to the SGWB (see e.g. Wang et al. 2019). Further, when we maximize the merger rate, we also maximize the contribution to the SGWB, so our optimal mass functions might run afoul of SGWB constraints at PBH abundances well below those excluded in other analyses.

### 3.1 Applying constraints to the mass function

In order to translate gravitational wave observables to discovery prospects and constraints on the population of DP black holes, we must alternately minimize and maximize the merger rate subject to particular constraints. This is similar to the problem of maximizing the overall abundance of black holes subject to observational constraints, as discussed by Lehmann et al. (2018). In that reference, the general form of the optimal mass function is derived analytically, and it is shown that the exact global optimum can be found semi-analytically with arbitrary precision. Since we will use some of the same methods and terminology, we briefly review this result. However, as we will explain, this formalism cannot be adapted to optimize the merger rate semi-analytically.

We treat observational constraints on the black hole population following Carr et al. (2017). In general, observational constraints on the black hole population are derived from some measured quantity $A_{\rm obs}$. The value of $A_{\rm obs}$ is predicted to be $A_0$ in the absence of any primordial black holes, whereas in the presence of PBH, one has $A_{\rm obs} = A_0 + A_1$. For most observables, black holes at different mass scales contribute independently, so we can write

$$A_1 = \int \mathrm{d}m\, \psi(m)\, K_1(m) \tag{18}$$

for some kernel $K_1(m)$. Provided that the constraining observable has this form, the constraint condition can be written in the form $C(\psi) \leq 1$, where $C(\psi)$ is the functional

$$C(\psi) \equiv \int \mathrm{d}m\, \frac{\psi(m)}{f_{\rm max}(m)}. \tag{19}$$

Here $f_{\rm max}(m)$ is the maximum allowed fraction of dark matter in the form of PBH assuming a monochromatic mass function at mass $m$. For the case of $N$ independent constraints $f_{{\rm max},j}(m)$, corresponding to a vector $C_j(\psi)$, this generalizes to

$$\left\|\vec{C}(\psi)\right\|^2 \equiv \sum_{j=1}^{N} \left( \int \mathrm{d}m\, \frac{\psi(m)}{f_{{\rm max},j}(m)} \right)^2 \leq 1. \tag{20}$$

Note, in particular, that $\psi(m) > f_{\rm max}(m)$ is perfectly admissible for a subset of masses—i.e., the mass function can cross through the curves on constraint plots—as long as the condition above is still met. This is simply because constraint curves, as typically drawn, are only applicable to monochromatic mass functions.

Since the total density in PBH scales linearly with the normalization of the mass function, any mass function can be normalized to saturate observational constraints, yielding the *normalized mass*, $\mathcal{M}(\psi) = \|\vec{C}(\psi)\|^{-1} \int \mathrm{d}m\, \psi(m)$. Finding the mass function which maximizes the PBH density subject to observational constraints is thus equivalent to maximizing the functional $\mathcal{M}$, which can be done semi-analytically.

One might hope that a similar method might apply to the optimization of the merger rate. But even if the merger rate functional were as simple as the normalized mass, it would still not be possible to apply the preceding formalism. As we have discussed, it is essential to consider constraints from non-detection of a stochastic gravitational wave background (SGWB) signal, but this constraint cannot be cast in the form of eq. (20). We now briefly review the nature and calculation of the SGWB constraint.

A population of primordial black holes produces a stochastic gravitational wave background from mergers at higher redshifts (Rosado 2011; Regimbau 2011; Zhu et al. 2011; Wang et al. 2018, 2019). While such backgrounds do not furnish a smoking-gun signal of a primordial origin for a particular black hole, they do constrain the PBH mass function. A differential merger rate $\mathcal{R}$ produces a stochastic background at frequency $\nu$ with density

$$\Omega_{\rm GW}(\nu) = \frac{\nu}{\rho_c} \int \mathrm{d}z\, \mathrm{d}m_1\, \mathrm{d}m_2\, \frac{\mathcal{R}(z; m_1, m_2)}{(1+z)H(z)} \times \frac{\mathrm{d}E_{\rm GW}}{\mathrm{d}\nu_s}(\nu_s; m_1, m_2), \tag{21}$$

where $\rho_c$ is the critical density and $\mathrm{d}E_{\rm GW}/\mathrm{d}\nu_s$ denotes the spectrum of the radiation emitted during a merger, with $\nu_s = (1+z)\nu$

denoting the frequency at the source. We follow the computation of the spectrum and the resulting $\Omega_{\rm GW}(\nu)$ in Zhu et al. (2011) and Wang et al. (2019). LIGO is most sensitive to the SGWB at a frequency of $\nu_p \sim 20\,\mathrm{Hz}$, and the sensitivity is sharply peaked around $\nu_p$. Thus, we determine whether a mass function is ruled out by SGWB production by simply comparing $\Omega_{\rm GW}(\nu_p)$ with LIGO constraints at that frequency, translating to the requirement that $\Omega_{\rm GW}(\nu_p) \lesssim 2 \times 10^{-9}$ (Wang et al. 2019).

Since the calculation of the SGWB is dependent on the shape of the entire mass function, this constraint cannot be expressed in the form of eq. (18). In particular, note that the strength of the constraint is not linear in the normalization of the mass function, since the merger rate itself depends on the normalization in a highly nonlinear fashion. There is no simple closed-form rescaling of the mass function that will saturate SGWB constraints. Practically, this is not an issue, since the optimal mass functions and the corresponding constraints on the black hole population must ultimately be derived numerically rather than analytically. In our numerical procedure, we can incorporate SGWB constraints on a nearly equal footing with other observational constraints, as we will explain in the following section.

### 3.2 Numerical procedure

We now detail the numerical procedure that we use to optimize the merger rate. We minimize and maximize the merger rate using simulated annealing (Kirkpatrick et al. 1983). In simulated annealing, at each step of the algorithm, a random modification to the state of the system is generated. Each modification is probabilistically accepted or rejected, and steps that decrease the cost function are preferentially accepted—i.e., simulated annealing is a Monte Carlo Markov chain (MCMC) optimization algorithm. Simulated annealing is structurally similar to the Metropolis–Hastings algorithm (Metropolis et al. 1953; Hastings 1970) for drawing samples from a distribution, but the probability of accepting a given step changes over time.

Heuristically, simulated annealing is based on an analogy to the physical process of annealing, in which a material is heated and then cooled slowly to relieve internal stresses. Heating allows the material to return to an equilibrium configuration, and since the cooling is slow, the material is likely to be in or near its equilibrium state once frozen. In simulated annealing, the system is first "heated" in the sense that random steps are accepted with a high probability. Then the temperature is slowly reduced, so that the system increasingly disfavors departure from equilibrium. This procedure locates global optima relatively efficiently: at first, while the system is "hot", the algorithm can generate a chain which explores the parameter space broadly, with little chance of being stuck at a local optimum. As the system cools, the chain is less likely to depart from a local optimum, so it tends to locate that optimum more precisely with subsequent steps.

#### 3.2.1 *The annealing algorithm*

The simulated annealing procedure is outlined in algorithm 1. The mass function $\psi(m)$ is binned into a set of values $\psi_i$ with bin widths $\Delta m_i$, so that $f_{\rm PBH} = \sum_i^N \psi_i \, \Delta m_i$.

The number of mass bins, $N$, must be large enough to allow for sufficient flexibility in the mass function, but must not be so large as to make the calculation intractable. The computational cost of the merger rate calculation scales asymptotically as a power law in $N$, but more importantly, each additional mass bin constitutes an additional dimension for the optimization problem. Naively, since the size of a discretized search space scales exponentially with the number of dimensions, one expects a similar behavior for the number of steps to convergence of the optimization algorithm, i.e., $n_{\rm steps} \sim b^N$. If the exponential base $b$ were large, the numerical optimization we attempt here would be extremely challenging. Pragmatically, since values of the mass function in adjacent bins are highly correlated, $b$ is manageably small: in direct numerical experiments, by subdividing mass bins, we find that $b \sim 1.5$. We choose $N = 21$, dividing the bins into three regions. We use 13 bins for $m < m_{\rm DP}^{\rm min}$, 5 bins for $m_{\rm DP}^{\rm min} < m < m_{\rm DP}^{\rm max}$, and 3 bins for $m > m_{\rm DP}^{\rm max}$, subdividing each region into equally-sized logarithmic bins. This makes it feasible for us to generate the numerical results in this work with $O(10^4)$ CPU hours.

The probability of accepting ("jumping" to) the candidate step, $P_{\rm jump}$, is defined by

$$P_{\rm jump} = \left[\texttt{cost}(\psi')/\texttt{cost}(\psi)\right]^{-1/T}, \tag{22}$$

where `cost` represents the functional to be minimized, and $T$ is the "temperature". In the simplest case, `cost` is the DP merger rate (for minimization) or its negative (for maximization). In our case, where the optimization problem is constrained, it is convenient to implement these constraints by adding terms to the cost function. Constraints appear in the cost function with a factor of $1/T$ so that, as the temperature drops, constraints become more important. Thus, our cost function is defined by

$$\texttt{cost}\,(\psi) = \pm R_{\rm DP}(\psi) + \frac{\beta}{T} \max\{0, \mathcal{P}(\psi)\}, \tag{23}$$

where the penalty functional $\mathcal{P}$ is defined by

$$\mathcal{P}(\psi) = \exp\left(\max\left\{\left\|\vec{C}(\psi)\right\|, \; \Omega_{\rm GW}/\Omega_{\rm GW}^{\rm max}\right\} - 1\right) - 1, \tag{24}$$

with $\vec{C}(\psi)$ defined as in eq. (20). We choose $\beta = 10^3\,\mathrm{yr}^{-1}$ so that even when the merger rate is at its maximum, the penalty functional still dominates the cost at the lowest temperatures we consider.

In addition, there are three components of the simulated annealing algorithm which must be implemented in a manner specific to each application: the selection of the initial point, the generation of new steps, and the cooling rate (annealing schedule).

To start new chains, we determine the initial mass function $\psi_0$ by choosing a random value in each mass bin from the log-uniform distribution on $[1, 10^3]$. The resulting mass function is then rescaled to match the input values of $r_{\rm DP}$ and $f_{\rm PBH}$. The generation of new steps is represented by the NEIGHBOR function, which mutates the current state of $\psi$ to obtain a candidate $\psi'$. The behavior of NEIGHBOR is specified in algorithm 2. Schematically, a step is generated by modifying the value of $\psi$ in a randomly-selected bin $i$. The modification is drawn from a normal distribution with mean $\psi_i$ and standard deviation $\sigma\psi_i/\Delta m_i$. Appropriate sections of the resulting mass function are then rescaled to match the input $r_{\rm DP}$ and $f_{\rm PBH}$.

We use a modified exponential cooling schedule, with a lower limit of $T = 1$. The temperature at the $k$th step is thus

$$T(k) = 1 + (T_0 - 1)(1 - \alpha)^k, \tag{25}$$

where we set $\alpha = 10^{-2}$, and $T_0$ is the initial temperature. In general, $T_0$ must be chosen empirically to allow the algorithm to explore a wide parameter space initially. We choose the initial temperature so that 80% of steps from the initial position which increase the cost are accepted. Such a temperature is high enough to "melt" the

**Algorithm 1** Annealing procedure

$k \leftarrow 0, \psi \leftarrow \psi_0$
**while** $k < k_{\max}$ **do**
  $\psi' \leftarrow \textsc{neighbor}(\psi)$ ▷ Generate modification
  **if** $P_{\rm jump}(\psi', T(k)) > \texttt{random}((0,1))$ **then**
    $\psi \leftarrow \psi'$ ▷ Accept modification
    $k = k + 1$
  **end if**
**end while**

**Algorithm 2** Neighbor generation

**procedure** $\textsc{neighbor}(\psi)$
  $\psi' \leftarrow \psi$
  $i \leftarrow \texttt{random}(\{1, 2, \ldots, N_{\rm bins}\})$ ▷ Choose bin
  $\psi_i' \leftarrow \psi_i \times \texttt{normal}(\psi_i, \sigma\psi_i/\Delta m_i)$ ▷ Modify bin
  $I \leftarrow \sum_i \psi_i \Delta m_i$ ▷ Fix $r_{\rm DP}$
  $I_{\rm DP} \leftarrow \sum_{i \in {\rm DP}} \psi_i \Delta m_i$
  **for** $i \in$ DP **do**
    $\psi_i' \leftarrow \psi_i' \times r_{\rm DP}(I - I_{\rm DP})/[I_{\rm DP}(1 - r_{\rm DP})]$
  **end for**
  $I \leftarrow \sum_i \psi_i \Delta m_i$ ▷ Fix $f_{\rm PBH}$
  **for** $i = 1, \ldots, N_{\rm bins}$ **do**
    $\psi_i' \leftarrow \psi_i' \times f_{\rm PBH}/I$
  **end for**
**end procedure**

system, allowing almost any step to proceed, while still being low enough that steps will be constrained as the temperature is lowered.

To verify convergence, we optimize the mass function five times, i.e., with five independent chains, at each parameter point. We evolve each chain for $10^7$ steps. Each of these chains begins with its own random mass function and with a high temperature, so convergence to the same optimum merger rate and mass function provides reassuring evidence that the algorithm is not stochastically settling into local optima. We find empirically that the merger rate typically converges across the chains within $O(10^5)$ steps.

### 3.2.2 *Two-parameter optimization*

Our goal is to determine the maximum and minimum merger rates as a function of the total abundance of PBH, $f_{\rm PBH}$, and the fraction of those PBH which lie in the DP mass range, $r_{\rm DP}$. Thus, in principle, we must perform the optimization described in the previous section at every point in this parameter space, independently. However, the optimization process is computationally expensive, so it cannot be applied directly to a fine grid in $(r_{\rm DP}, f_{\rm PBH})$. Instead, we use the simulated annealing algorithm on a coarse grid, and then use an alternative technique to interpolate between the resulting optima.

First, we note that this interpolation process is not simply an aesthetic matter. In principle, a small displacement in the $(r_{\rm DP}, f_{\rm PBH})$ plane can produce a sharp discontinuity in the shape of the optimal mass function, leading to discrete regions in which the optimal mass function evolves very differently with $r_{\rm DP}$ and $f_{\rm PBH}$. This is especially difficult to forecast when observational constraints are included. The situation is analogous to the behavior of the order parameter in a first-order phase transition: in this case, a small displacement in temperature discontinuously changes the location of the minimum of the free energy. In our case, rather than a sharp transition between two minima of the free energy, there could be a sharp transition between two shapes of the mass function. A naive interpolation of a coarse grid of points risks missing any such structure.

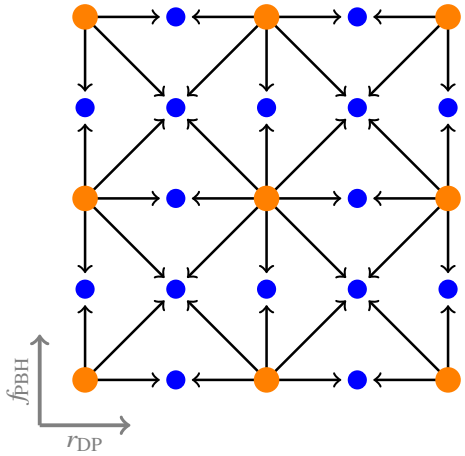



**Figure 3.** Illustration of the refinement procedure. Orange points represent a subset of the initial grid. Blue points are those added during the refinement step. An arrow from an orange point to a blue point denotes that a chain is initialized at the blue point using the optimal mass function across all chains previously evaluated at the orange point.

Therefore, we extend our coarse grid to a finer subgrid using the following procedure. First, each interval in the grid is halved to produce a refined grid. The initial mass functions for each new point on the grid are borrowed from its nearest neighbors: that is, for each neighbor, we run an independent chain at the new parameter point starting from the neighbor's optimal mass function across all of the neighbor's chains. One step of the process is illustrated in fig. 3. Even if there is a transition of the kind described above between the new point and some of its neighbors, it is still likely that the optimum at the new point is close in shape to that of at least one neighbor. Thus, one expects that only mild adjustment of these mass functions is needed to converge to the optimum at the new point.

Since we assume that at least one of the optimal mass functions drawn from the neighboring points is close to the global optimum of the new point, there is no need for the variable temperature of simulated annealing: we need only locate the nearby optimum more precisely. We perform this adjustment by producing a chain of $10^5$ steps with the Metropolis–Hastings algorithm, which is structurally similar to simulated annealing, but with a fixed temperature. We perform the entire grid refinement procedure twice to obtain a sufficiently fine grid.

Finally, the optima from all points are "mixed" as follows. For each point on the refined grid, we generate another set of $10^5$-step Metropolis–Hastings chains, each with a different initial mass function. One chain begins with the optimal mass function from the point itself. Another chain is initialized from the optimal mass function of each nearest neighbor. The mixing process is performed four times, so an optimal mass function shape found at any point in a block between initial grid points can propagate to other points in the same block.

After the refinement and mixing processes are performed, the result is a non-trivial interpolation of the initial grid, which forms the basis for our results in the following sections.

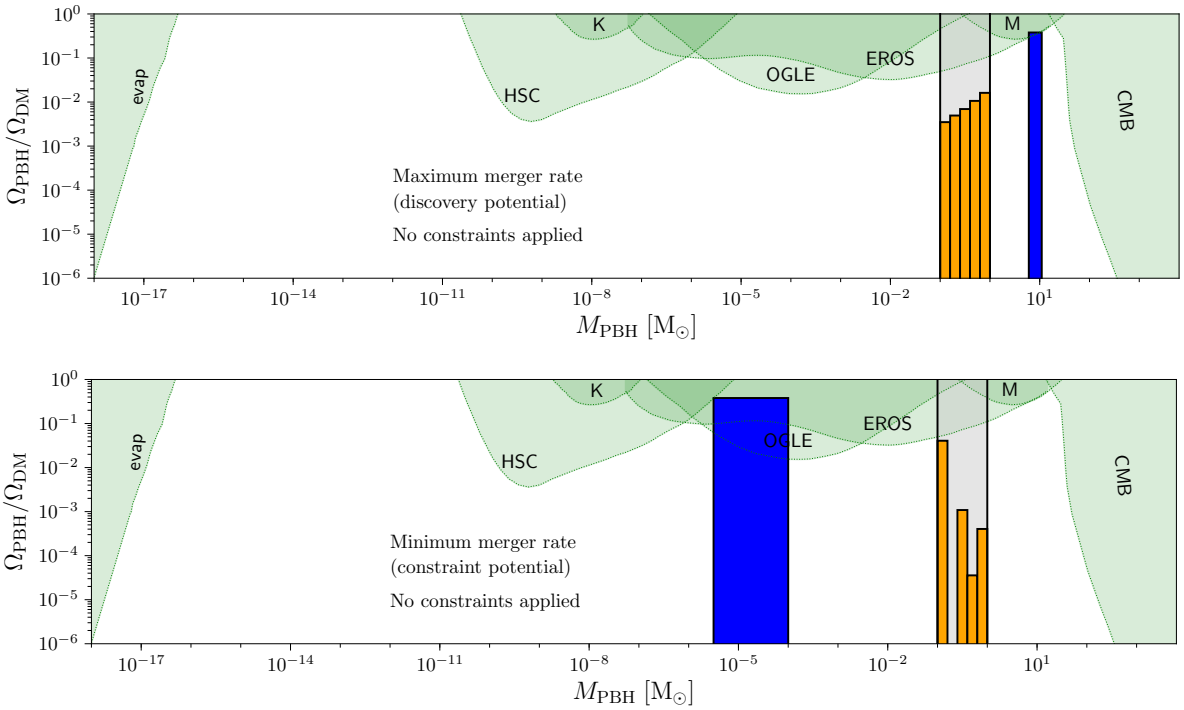



**Figure 4.** Optimal maximizing (top) and minimizing (bottom) mass functions with $f_{\rm PBH} = 0.5$ and $r_{\rm DP} = 0.1$ in the absence of observational constraints. Each mass function is shown as a set of discrete bars with height $\Omega_{\rm PBH}(m_i)/\Omega_{\rm DM} \equiv \psi(m_i)\Delta m_i$, i.e., the height of each bar indicates the total mass in the bin. The maximum merger rate corresponds to the most optimistic discovery potential, and the minimum merger rate to the most pessimistic constraint potential. The constraint curves are *not* used to constrain the mass function, and are shown here only for reference and comparison with fig. 5. The DP window is indicated by the shaded gray region, and the mass function is colored orange therein. The labeled constraints are from BH evaporation (`evap`, Carr et al. (2010)), Hyper Suprime-Cam (`HSC`, Niikura et al. (2019); Smyth et al. (2020)), Kepler (`K`, Griest et al. (2014)), OGLE (`Ogle`, Wyrzykowski et al. (2011)), EROS-II (`EROS`, Tisserand et al. (2007)), MACHO (`M`, Allsman et al. (2001)), and CMB observables (`CMB`, Ali-Haïmoud & Kamionkowski (2017); Carr et al. (2017)). Other constraints may also apply, but their inclusion does not influence our qualitative conclusions (see section 3).

## 4 RESULTS

We now examine the results of our numerical optimization. First we show results for individual parameter points, and compare the shapes of optimal mass functions to our analytical expectations. Then we show minimal and maximal merger rates with and without observational constraints.

### 4.1 Shape of the mass function

To understand the shapes of the mass functions which optimize the merger rate, we first neglect observational constraints to facilitate comparison with the analysis in section 2.3. Figure 4 shows mass functions which minimize and maximize the merger rate without regard to observational constraints for the parameter point $(r_{\rm DP}, f_{\rm PBH}) = (0.1, 0.5)$ (i.e., 50% of DM is in PBH of any mass, and 10% of the PBH density is accounted for by the DP window). The two mass functions are mostly distinguished by two features. First, they have clearly different behavior outside the DP window: the DP merger rate is enhanced when the remainder of the PBH are placed at a higher mass, above the top of the window, and it is reduced when they are placed at lower mass, below the bottom of the window. Second, as expected from our simplified analysis in section 2.3, the maximizer is broad within the DP window, while the minimizer is sharply peaked and multimodal.

Contrary to our naive expectation, the maximizer prefers higher masses within the DP window, while the minimizer prefers lower masses. This is because the full numerical calculation accounts for detectability, and the mergers of heavier black holes are detectable in a larger volume. This also accounts for the behavior of the mass function outside the DP window. Recall that the mergers of DP black holes with *heavier* black holes are generally observable, and we assume that the lighter black hole is identifiably primordial in such a merger. However, the merger of a DP black hole with a *lighter* black hole may not be observable, or may be observable only in such a small effective volume that our assumptions for calculating the merger rate are not valid. Thus, if the 90% of PBH which lie outside the DP window are positioned at higher masses, the observable merger rate is enhanced.

Having noted the behavior of the optimal mass functions in the absence of observational constraints, we now turn to the results of constrained optimization in fig. 5. The general features of these optima are similar to their unconstrained counterparts, and observational constraints modify the shapes of the optimal mass functions in a comprehensible manner. The maximal merger rate is still obtained with additional PBH positioned above the DP window, but observational bounds now strictly constrain the position of this peak. The mass function which minimizes the merger rate is not subject to strong constraints within the DP window, but the additional PBH at lower masses must now be repositioned to the mass range where constraints are weaker.

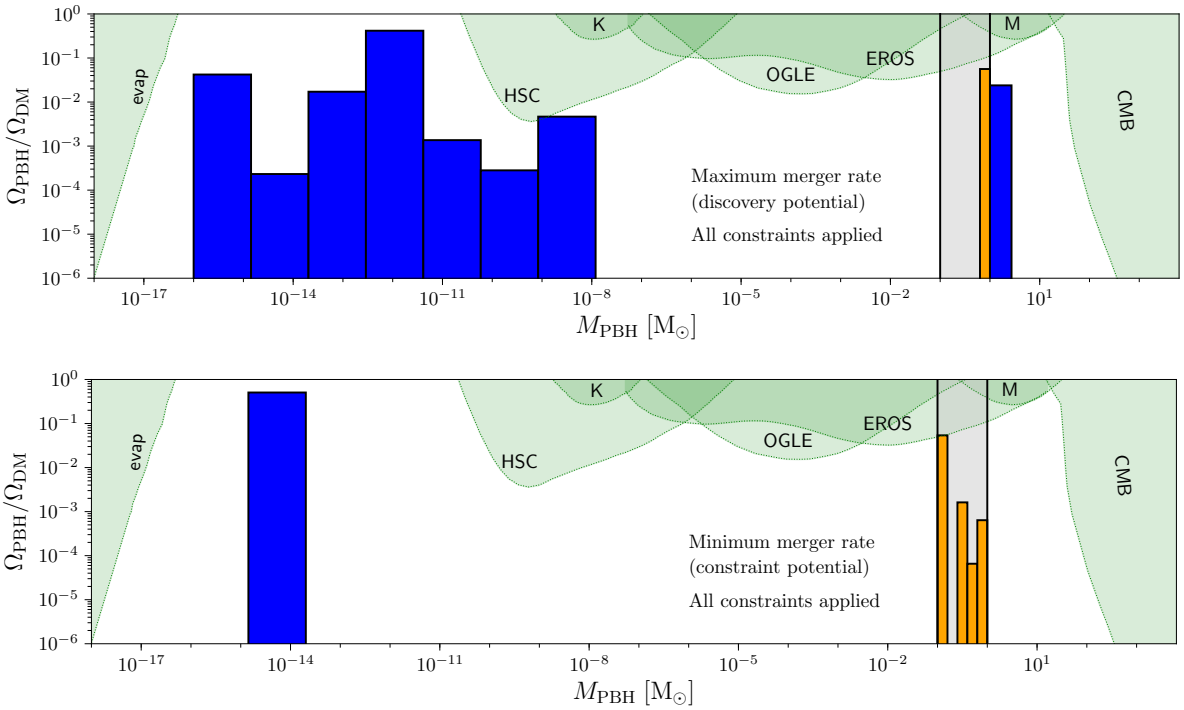



**Figure 5.** Optimal maximizing (top) and minimizing (bottom) mass functions with $f_{\rm PBH} = 0.5$ and $r_{\rm DP} = 0.1$. Each mass function is shown as a set of discrete bars with height $\Omega_{\rm PBH}(m_i)/\Omega_{\rm DM} \equiv \psi(m_i)\Delta m_i$, i.e., the height of each bar indicates the total mass in the bin. All observational constraints are applied. The maximum merger rate corresponds to the most optimistic discovery potential, and the minimum merger rate to the most pessimistic constraint potential. The DP window is indicated by the shaded gray region, and the mass function is colored orange therein. The labeled constraints are from BH evaporation (`evap`, Carr et al. (2010)), Hyper Suprime-Cam (`HSC`, Niikura et al. (2019); Smyth et al. (2020)), Kepler (`K`, Griest et al. (2014)), OGLE (`Ogle`, Wyrzykowski et al. (2011)), EROS-II (`EROS`, Tisserand et al. (2007)), MACHO (`M`, Allsman et al. (2001)), and CMB observables (`CMB`, Ali-Haïmoud & Kamionkowski (2017); Carr et al. (2017)). Other constraints may also apply, but their inclusion does not influence our qualitative conclusions (see section 3).

### 4.2 Constraints and discovery prospects

Minimum and maximum merger rates with all constraints applied are shown as a function of $r_{\rm DP}$ and $f_{\rm PBH}$ in figs. 6 and 7. The minimum merger rate corresponds to LIGO's constraint potential: even given complete freedom in the mass function, there is no way to obtain a lower observable merger rate. The maximum merger rate corresponds to the discovery potential, i.e., the most optimistic scenario given any mass function.

The light gray region in the top-right corner of each panel indicates parameter points where the numerical procedure was unable to locate any mass function consistent with constraints. This is the portion of parameter space which is already ruled out by other observables, including the stochastic gravitational wave background (SGWB). The extent of this region can be estimated using the semi-analytical procedure of Lehmann et al. (2018), which can give the maximum allowed value of $f_{\rm PBH}$ for fixed $r_{\rm DP}$ if SGWB is neglected. This bound is the triangular dark gray region. Since the SGWB depends non-linearly on the mass function, it cannot be treated within the same semi-analytical framework. Thus, one expects the light gray region to extend slightly further than the dark gray region, which is exactly the behavior shown in figs. 6 and 7.

Observe that there is a small gap between the minimum and maximum merger rates when $r_{\rm DP}$ is near 1. This is simply because there is very limited freedom in the mass function under these conditions. On the other hand, when $r_{\rm DP} \ll 1$, the minimum and maximum merger rates are radically different. In particular, while LIGO can only rule out mass functions with $r_{\rm DP} \gtrsim 0.1$, it can potentially discover PBH with only $r_{\rm DP} \gtrsim 10^{-4}$ with $O(1\,\mathrm{yr})$ of data. The effect of observational constraints is evident from fig. 8: in the absence of constraints, LIGO would potentially be sensitive to mergers of a subcomponent as small as $r_{\rm DP} \sim 10^{-6}$.

### 4.3 Convergence

For an optimization problem of this kind, which is not generally convex, there is no reliable test of algorithmic convergence. In principle, it is always possible that the loss landscape has not been fully explored, and that in some corner, there is a point which outperforms the optima that we have discovered numerically. The best defense against this issue is to compare the numerical results against simplified analytical benchmarks, as we have carried out above.

However, we also perform two more direct tests of convergence. First, we have verified that we locate the global optimum in a low-dimensional example, where the features of the loss function can be analyzed by inspection; and second, we perform a purely numerical test of convergence by comparing the results of many MCMC chains initialized in random configurations. We thus check directly that at benchmark points, all of our chains converge to the same merger rate within our fixed step count.

Numerical convergence is also supported qualitatively by comparison of nearby parameter points. Since we perform the optimization procedure on a grid of points in the $(r_{\rm DP}, f_{\rm PBH})$ plane, nearest neighbors in this plane should converge to similar optima. Since the contours in figs. 6 and 7 are smooth, one might conclude that this constitutes evidence of convergence. However, note that in figs. 6

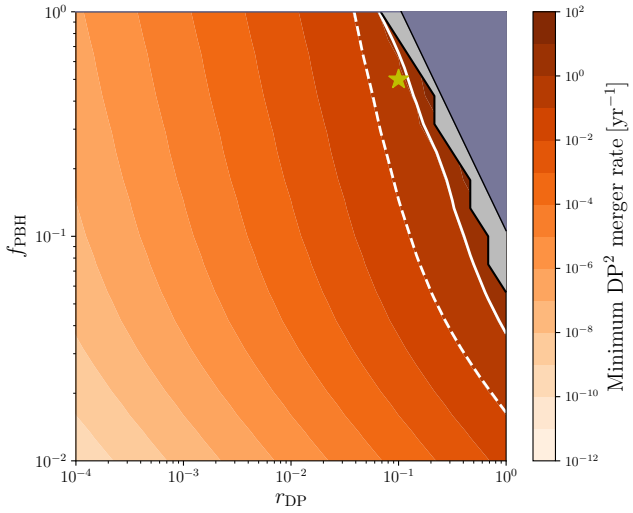



**Figure 6.** Minimum DP merger rate for mass functions constrained by all observables, including SGWB. The triangular region at the top-right is ruled out by non-GW observables. The light region is ruled out by the combination of all observables. The solid and dashed curves show contours with an *observed* DP merger rate of 1 yr$^{-1}$ and 0.1 yr$^{-1}$, respectively. The star (★) indicates the point shown in the bottom panel of fig. 5.

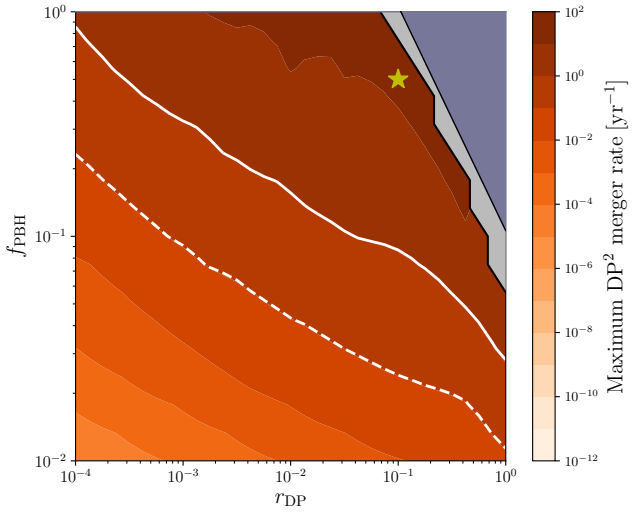



**Figure 7.** Maximum DP merger rate for mass functions constrained by all observables, including SGWB. The triangular region at the top-right is ruled out by non-GW observables. The light region is ruled out by the combination of all observables. The solid and dashed curves show contours with an *observed* DP merger rate of 1 yr$^{-1}$ and 0.1 yr$^{-1}$, respectively. The star (★) indicates the point shown in the top panel of fig. 5.

and 7, optima from an initial run have been mixed between parameter points, as described in section 3.2.2. In particular, if a global optimum is discovered at only one point, it will subsequently propagate to the rest of the parameter space, even if chains originally produced elsewhere located very different optima. Thus, smoothness of the contours is only meaningful before mixing. Since the initial grid with random priors is relatively sparse, smoothness is difficult to assess quantitatively. However, we have verified that the qualitative features of the contours in figs. 6 and 7 are not affected by the mixing procedure, suggesting that each of the points in the initial grid is locating nearly the same optimum as that produced after mixing. Note that the sharp behavior at the top of fig. 7 is entirely due to observational constraints, and disappears in their absence.

## 5 DISCUSSION AND CONCLUSIONS

The discovery of primordial black holes would be a tremendous step forward in our understanding of cosmology. If PBH exist, they encode information about cosmic history in an epoch that we have yet to probe observationally. They also provide an empirical test of physics at extremely high scales and early times. Moreover, despite all observational constraints, PBH remain a viable and extremely simple candidate for cosmological dark matter.

Conveniently, any black hole with a mass below $\sim 1\,M_\odot$ cannot have an astrophysical origin. Gravitational wave observatories are well-suited to identify black holes and to measure their masses precisely, so these instruments can detect a smoking-gun signature of the existence of PBH. Even one detection event involving a light black hole would provide unambiguous evidence for new physics. Subsequent exploration of the abundance and distribution of such black holes would test the possible formation scenarios, and potentially provide a direct handle on physics at very early times.

The problem lies in the interpretation of a null observational result. In principle, experimental results at LIGO constrain the population of light PBH, and in principle, again, LIGO may be sensitive to a very small abundance of such objects. However, both of these statements have a non-trivial dependence on the shape of the PBH mass function. Since the merger rate has a complicated non-linear dependence on the mass function, it is difficult to directly assess the significance of this uncertainty. In particular, the semi-analytical analysis of Lehmann et al. (2018) cannot accommodate the merger rate as a constraint on the PBH abundance.

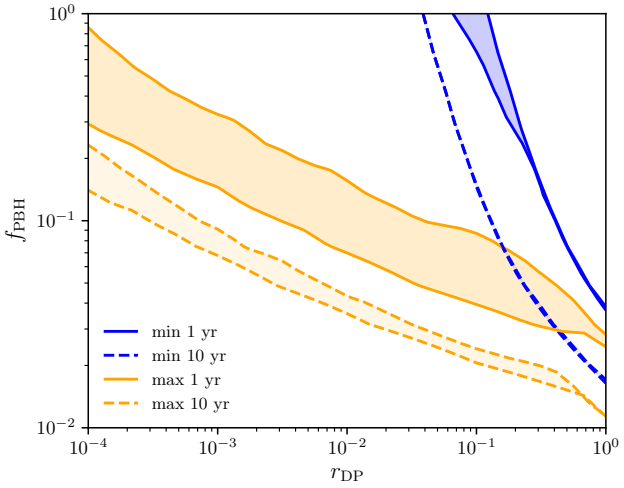



**Figure 8.** Contours with DP merger rate fixed to 1 yr$^{-1}$ (solid) and 0.1 yr$^{-1}$ (dashed), with and without observational constraints. The bottom of each band shows the sensitivity with complete freedom in the mass function, and the top shows the sensitivity when observational constraints are included. Blue curves show the minimum merger rate, corresponding to the constraint potential. Note that the 10-year minimum curves with and without constraints are essentially identical.

In this work, we have quantified the uncertainty in the PBH merger rate that arises from freedom in the mass function, while accounting for observational constraints that restrict its shape. This uncertainty is reflected in the gap between the minimum-rate and maximum-rate contours in fig. 8. While the two bands are not far apart for $r_{\rm DP} \sim 1$, they are significantly different when $r_{\rm DP} \ll 1$. Thus, it is necessary to consider the two contours as reflecting different notions of experimental sensitivity at LIGO. The minimal merger rate determines the extent of constraints that LIGO can set, if the mass function is allowed to vary freely. Conversely, the maximal merger rate determines the extent of the parameter space that can be probed by LIGO in the most optimistic scenario.

Our numerical results indicate that LIGO's constraint potential is limited to parameter space with $r_{\rm DP} \gtrsim 0.1$, and the prospects for improving this bound with binary black hole mergers are limited. On the other hand, LIGO's discovery potential extends as low as $r_{\rm DP} \sim 10^{-4}$, meaning that even a very small subcomponent of the PBH population that lies in our DP window can potentially yield a detection. This also establishes the relevance of constraints provided by other observables: in the absence of observational constraints, LIGO would be sensitive to $r_{\rm DP} \sim 10^{-6}$. Our results highlight the importance of evaluating detection prospects for specific PBH models using the full apparatus of the merger rate for extended mass functions—a small subcomponent of DPBH cannot be neglected.

One might wonder whether the optimal mass functions we consider in this work are realistic. Generally, there is good motivation to consider only specific forms of the mass function, particularly monochromatic, lognormal, or power-law shapes. However, most of the behavior that characterizes our optimal mass functions is captured by doubly- or triply-peaked mass functions, and note that a population of PBH with a multimodal mass function can easily be generated after inflation (Carr & Kuhnel 2019). Thus, while the exact form of our optimal mass functions might require fine tuning of initial conditions, approximate forms which retain a high or low merger rate are much more generic. The non-trivial requirement is that a peak should fall near the DP window to maximize discovery prospects. As yet, there is no direct evidence for such placement, but only circumstantial evidence from the distribution of mergers observed thus far.

Our results are inherently subject to theoretical uncertainties in the computation of the merger rate. While the form of the merger rate employed here reflects the current state of the art, such formulae are best suited only to computations at the order of magnitude level. For instance, one potential issue in the rate calculation is the effect of other black holes in disrupting the formation of a binary. In our calculation, as discussed by Chen & Huang (2018), we assume that two black holes of mass $m_i$ and $m_j$ do not form a binary if another black hole of mass $m_k \geq \min\{m_i, m_j\}$ is present in the volume between them. However, even if this were always the case, it is also possible that somewhat lighter black holes would have a similar effect. This would provide a mechanism for suppression of the merger rate, weaking the constraint we draw in this work. However, our qualitative results stand even if the merger rate is correct only at the order-of-magnitude level. In particular, the gap between the maximal and minimal merger rates is very large at small $r_{\rm DP}$, and is robust to adjustments in the calculation of the merger rate.

The stochastic gravitational wave background (SGWB) associated with mergers over cosmic time may provide an additional probe of the PBH abundance. We do not evaluate SGWB as a discovery mechanism in this work simply because such a detection would not constitute unambiguous evidence of new physics. It is possible that features of the SGWB may be connected to the features of the PBH population with enough precision to empirically test specific models, but since other physical mechanisms might contribute to the SGWB, substantial follow-up work would be required to confirm the existence of a population of PBH. One might think that any mass function tuned for an enhanced merger rate would contribute a great deal to the SGWB, and thus, while we do not examine the SGWB as a tool for discovery, we do consistently include this observable as one of our constraints on the mass function. All of the constrained optima considered in this work, including those with maximal merger rates, are compatible with existing SGWB constraints. Significant improvement of constraints on the SGWB might limit freedom in the mass function, and might thus limit the discovery potential we infer in this work.

Our results show that while LIGO has limited power to constrain the abundance of light PBH, it nonetheless has significant discovery potential. The major obstruction to such sensitivity is not the sensitivity of the LIGO instrument, but the analysis pipeline. There are significant computational costs to conducting searches for mergers of light black holes, as discussed extensively by Magee et al. (2018), and these costs increase further if one searches for mergers of light black holes with heavier black holes. However, the freedom in the mass function and the associated uncertainty in the merger rate provides ample motivation for the refinement of methods for such searches, and even for the dedication of additional computational resources. A single observation of this type would have immense value, and gravitational wave observatories are in a unique position to make such a discovery.

## ACKNOWLEDGEMENTS

BVL and SP are partially supported by the U.S. Department of Energy grant number de-sc0010107. We acknowledge valuable conversations with Nergis Mavalvala and Sarah Shandera. This work made use of the Hummingbird Computational Cluster operated by UC Santa Cruz Research Computing, and we thank the Research Computing staff for valuable support.

## REFERENCES

Abbott B., et al., 2005, Phys. Rev., D72, 082002
Abbott B., et al., 2009, Nature, 460, 990
Abbott B., et al., 2016a, Phys. Rev. X, 6, 041015
Abbott B., et al., 2016b, Phys. Rev. Lett., 116, 061102
Abbott B., et al., 2016c, Phys. Rev. Lett., 116, 221101
Abbott B. P., et al., 2016d, Phys. Rev. Lett., 116, 241103
Abbott B. P., et al., 2017a, Phys. Rev. Lett., 118, 121101
Abbott B. P., et al., 2017b, Phys. Rev. Lett., 118, 221101
Abbott B., et al., 2017c, Phys. Rev. Lett., 119, 141101
Abbott B., et al., 2017d, Phys. Rev. Lett., 119, 161101
Abbott B., et al., 2017e, Astrophys. J. Lett., 848, L12
Abbott B., et al., 2017f, Astrophys. J. Lett., 848, L13
Abbott B. P., et al., 2017g, Astrophys. J., 851, L35
Abbott B., et al., 2019a, Phys. Rev. X, 9, 031040
Abbott B., et al., 2019b, Phys. Rev. Lett., 123, 161102
Abbott R., et al., 2020a
Abbott B., et al., 2020b, Astrophys. J. Lett., 892, L3
Abbott R., et al., 2020c, Astrophys. J., 896, L44
Ali-Haïmoud Y., Kamionkowski M., 2017, Phys. Rev. D, 95, 043534
Allsman R., et al., 2001, Astrophys. J. Lett., 550, L169
Bailyn C. D., Jain R. K., Coppi P., Orosz J. A., 1998, Astrophys. J., 499, 367

Bird S., Cholis I., Muñoz J. B., Ali-Haïmoud Y., Kamionkowski M., Kovetz E. D., Raccanelli A., Riess A. G., 2016, Phys. Rev. Lett., 116, 201301
Brandt T. D., 2016, Astrophys. J. Lett., 824, L31
Calmet X., Carr B., Winstanley E., 2014, Quantum Black Holes. Springer-Briefs in Physics, Springer, Berlin, doi:10.1007/978-3-642-38939-9
Capela F., Pshirkov M., Tinyakov P., 2013, Phys. Rev. D, 87, 123524
Carr B. J., 2003, Lect. Notes Phys., 631, 301
Carr B., Kuhnel F., 2019, Phys. Rev. D, 99, 103535
Carr B., Kuhnel F., 2020
Carr B., Kohri K., Sendouda Y., Yokoyama J., 2010, Phys. Rev. D, 81, 104019
Carr B., Kuhnel F., Sandstad M., 2016, Phys. Rev. D, 94, 083504
Carr B., Raidal M., Tenkanen T., Vaskonen V., Veermäe H., 2017, Phys. Rev. D, 96, 023514
Carr B., Kohri K., Sendouda Y., Yokoyama J., 2020
Chandrasekhar S., 1931, Astrophys. J., 74, 81
Chapline G. F., 1975, Nature, 253, 251
Chen Z.-C., Huang Q.-G., 2018, Astrophys. J., 864, 61
Chen Z.-C., Huang Q.-G., 2019
Clesse S., García-Bellido J., 2017, Phys. Dark Univ., 18, 105
Coughlin M. W., Dietrich T., 2019, Phys. Rev. D, 100, 043011
Farr W. M., Sravan N., Cantrell A., Kreidberg L., Bailyn C. D., Mandel I., Kalogera V., 2011, Astrophys. J., 741, 103
Fernandez N., Profumo S., 2019, JCAP, 08, 022
Gerosa D., Berti E., 2017, Phys. Rev. D, 95, 124046
Graham P. W., Rajendran S., Varela J., 2015, Phys. Rev. D, 92, 063007
Griest K., Cieplak A. M., Lehner M. J., 2014, Astrophys. J., 786, 158
Hassall J., 1904, The Old Nursery Stories and Rhymes. Blackie & Son
Hastings W., 1970, Biometrika, 57, 97
Hawking S., 1971, Monthly Notices of the Royal Astronomical Society, 152, 75
Inomata K., Kawasaki M., Mukaida K., Yanagida T. T., 2018, Phys. Rev. D, 97, 043514
Katz A., Kopp J., Sibiryakov S., Xue W., 2018, JCAP, 12, 005
Khlopov M. Y., 2010, Res. Astron. Astrophys., 10, 495
Kirkpatrick S., Gelatt C., Vecchi M., 1983, Science, 220, 671
Koushiappas S. M., Loeb A., 2017, Phys. Rev. Lett., 119, 041102
Lehmann B. V., Profumo S., Yant J., 2018, JCAP, 1804, 007
Magee R., et al., 2018, Phys. Rev., D98, 103024
Mandic V., Bird S., Cholis I., 2016, Phys. Rev. Lett., 117, 201102
Metropolis N., Rosenbluth A., Rosenbluth M., Teller A., Teller E., 1953, J. Chem. Phys., 21, 1087
Monroy-Rodríguez M. A., Allen C., 2014, Astrophys. J., 790, 159
Montero-Camacho P., Fang X., Vasquez G., Silva M., Hirata C. M., 2019, JCAP, 08, 031
Niikura H., et al., 2019, Nature Astron., 3, 524
Ozel F., Psaltis D., Narayan R., McClintock J. E., 2010, Astrophys. J., 725, 1918
Ozel F., Psaltis D., Narayan R., Villarreal A. S., 2012, Astrophys. J., 757, 55
Raidal M., Vaskonen V., Veermäe H., 2017, JCAP, 1709, 037
Regimbau T., 2011, Res. Astron. Astrophys., 11, 369
Rosado P. A., 2011, Phys. Rev. D, 84, 084004
Sasaki M., Suyama T., Tanaka T., Yokoyama S., 2016, Phys. Rev. Lett., 117, 061101
Shandera S., Jeong D., Gebhardt H. S. G., 2018, Phys. Rev. Lett., 120, 241102
Smyth N., Profumo S., English S., Jeltema T., McKinnon K., Guhathakurta P., 2020, Phys. Rev. D, 101, 063005
Soares-Santos M., et al., 2017, Astrophys. J. Lett., 848, L16
Sugiyama S., Kurita T., Takada M., 2020, Mon. Not. Roy. Astron. Soc., 493, 3632
Tisserand P., et al., 2007, Astron. Astrophys., 469, 387
Vaskonen V., Veermäe H., 2020, Phys. Rev. D, 101, 043015
Wang S., Wang Y.-F., Huang Q.-G., Li T. G. F., 2018, Phys. Rev. Lett., 120, 191102
Wang S., Terada T., Kohri K., 2019, Phys. Rev., D99, 103531
Wyrzykowski L., et al., 2011, Mon. Not. Roy. Astron. Soc., 416, 2949
Zel'dovich Y. B., Novikov I. D., 1967, Soviet Ast., 10, 602
Zhu X.-J., Howell E., Regimbau T., Blair D., Zhu Z.-H., 2011, Astrophys. J., 739, 86
Zumalacarregui M., Seljak U., 2018, Phys. Rev. Lett., 121, 141101
de Lavallaz A., Fairbairn M., 2010, Phys. Rev. D, 81, 123521

This paper has been typeset from a TEX/LATEX file prepared by the author.